Evaporation of Pinned Droplets Containing Polymer – An Examination of the Important Groups Controlling Final Shape

Adam D. Eales and Alexander F. Routh
Dept. of Chemical Engineering & Biotechnology, University of Cambridge, Cambridge, CB2 3RA, UK

Nick Dartnell and Simon Goddard
Cambridge Display Technology Ltd. (Company number 02672530), Godmanchester, PE29 2XG, UK

DOI 10.1002/aic.14777
Published online March 16, 2015 in Wiley Online Library (wileyonlinelibrary.com)

Controlling the final shape resulting from evaporation of pinned droplets containing polymer, is important in the fabrication of P-OLED displays by inkjet printing. Typically, a coffee - ring shape arises, due to the pinning and associated outward capillary flow. For operational reasons, this is undesirable – a flat topography is required. The aim of this work is to understand the important groups governing the shape, to provide a practical guide to ink selection. The theory presented is based on a thin-film lubrication model. The governing equations are solved numerically and continuously track the lateral progression of a liquid/gel front. A large capillary number or large ratio of initial to maximal polymer volume fraction can suppress the coffee-ring. White light interferometry is used to confirm these findings experimentally. © 2015 American Institute of Chemical Engineers *AIChE J*, 61: 1759–1767, 2015
Keywords: droplet, drying, capillary flow, coffee-ring, P-OLED

Introduction

There are a vast number of systems for which evaporation of a droplet, containing a nonvolatile component is relevant. The distribution of pesticide on leaves is important when attempting to kill weeds.[1] There are several biological applications, for example DNA microarrays,[2–5] blood residue analysis for disease diagnostics[6] and crime scene reconstruction.[7] In addition, drying is crucial to technologies using inkjet printing such as the fabrication of micro/nano electronics[8–12] and polymer-organic light-emitting diode displays (P-OLEDs).[13]

P-OLEDs are a technology in which light is emitted as a function of the electrical operation. Unlike existing display technologies, such as Liquid Crystal Displays (LCDs), they do not require a backlight with filters and they can be fabricated using a flexible and extremely thin substrate, rather than an inflexible layer of glass. For these reasons, they have the potential for much larger viewing angles and for use in the next generation of flexible electronics applications, such as curved television displays.

For P-OLED displays, a uniform final profile of the dried deposit is required, for operational reasons (see Figure 1). An undulating shape can occur, however, due to the coffee-ring effect.[14–17]

The coffee-ring effect occurs when the contact line between a droplet and substrate is "pinned," so that it does not advance nor recede. The cause of pinning can be due to either surface roughness, adsorption of the nonvolatile component or deposition of large particles in the vicinity of the contact line. An outward capillary flow arises and replenishes the liquid material evaporated near the contact line. This outward flow transports the nonvolatile material to the edge of the droplet, where it is deposited as a ring. Understanding and controlling this process is a problem which needs to be addressed and is the motivation for this article.

There have been several previous attempts to eliminate the coffee-ring effect. One can either try to prevent the droplet pinning or suppress the capillary flow. Adding a surfactant[1] can introduce a Marangoni flow which counteracts the outward capillary flow. Altering the pH[18,19] can influence the DLVO interactions and introduce an attraction between the nonvolatile component and the substrate, which dominates the capillary flow. Recently, it has been shown that through careful selection of an electric field, the coffee-ring can be suppressed.[20] Electrowetting[21] can be used to prevent pinning. Changing particle shape,[19,22,23] such as using ellipsoids rather than spheres, can also prevent coffee-ring formation. However, these approaches are not ideal for P-OLED applications.

The transport in, and residual patterns left by, droplets has been an area of significant research interest. There are a plethora of phenomena that can influence the dynamic behavior of the drying process. To predict the final profile, a numerical solution is invariably required. Instead of providing a comprehensive review of the literature, as in,[24,25] we will outline a few papers which have similarity to our theory and explain how our work differs.

There is significant debate about the exact nature of the evaporative flux distribution across a droplet. For the final shape, knowing the droplets' internal flow profile is important and this depends on the evaporative flux distribution.[26] A spatially uniform or edge enhanced evaporation profile

Correspondence concerning this article should be addressed to A. F. Routh at afr10@cam.ac.uk.

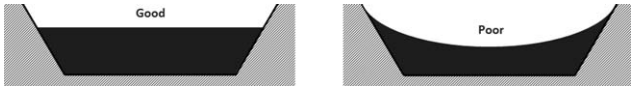

Figure 1. Sketch of typical pixel geometry. P-OLED displays contain many pixels.

During the manufacturing process an ink is jetted into each pixel. Following evaporation of the volatile component in the ink, the shape of the polymer residue can take different profiles, depending on the ink properties. It is desired to achieve a flat, rather than undulating, profile.

leads to an outward flow. If the evaporation is somehow enhanced at the center of the droplet, there is an inward flow. For large droplets with significant ventilation, one expects a uniform evaporation profile. For small droplets with stagnant surroundings, one expects larger evaporation toward the droplet edge. Many authors argue that when the atmosphere is stagnant and the liquid side mass transfer resistance is negligible, evaporation is controlled by diffusion of vapour away from the droplet surface.[27] Others consider an appreciable liquid side mass transfer resistance.[28] The general situation is not straight forward and it has been shown experimentally that for ambient conditions, the evaporative profile differs significantly from vapour diffusion models.[29] The purpose of our work is to provide a practical guide to controlling film shape. To that end, we are interested in the underlying trends relating the parameters of the system to the final shape. For this reason, the exact nature of the evaporative flux distribution will not greatly concern us but a couple of situations will be considered and we will show that it does not alter the trends in final film profile.

The work presented in this article has similarity to other thin-film lubrication models. Unlike the present research, the model of Ref. [20] considers both Marangoni flow and the presence of an electric field, in a cartesian coordinate system. The papers of Refs. [30] and [31] consider specific situations where a gel forms at a critical volume fraction of nonvolatile material and the gel then completely suppresses both flow and evaporation. We extend the situation to the case in which evaporation, though hindered, remains significant. Furthermore, rather than treating the position of the liquid/gel front as fixed on a lattice, we use a volume tracking argument to explicitly find its position at each time-step and hence track its propagation, continuously. Our results are presented over a broad range of polymer volume fractions, including very small polymer contents, at which we report some interesting phenomena. We also perform white light interferometry experiments, to verify the numerical findings.

The aim of this article is to uncover the governing groups that control the final film shape for inkjetted droplets of solvent containing light-emitting polymer, so that the coffee-ring effect can be minimized.

Mathematical Model

Assumptions and simplifications

We consider a droplet containing a single, volatile liquid (viscosity μ_0, surface tension γ_0), and a single, nonvolatile component (e.g. polymer) with initial volume fraction ϕ_0 (see Figure 2). It is assumed that the contact line remains pinned throughout the lifetime of the evaporation, either due to surface inhomogeneities on the substrate or to some adsorption of the nonvolatile material, at the edge. A cylindrical coordinate system is used and the droplet is assumed to be axisymmetric, such that angular velocity and gradients can be ignored ($v_\theta=0, \frac{\partial}{\partial\theta}=0$)

Typical droplet sizes are $\sim$125 μm in radius, R. Therefore, it is reasonable to ignore gravitational effects on the droplet interface compared to surface tension effects because the Bond number (Bo) is small.

$$Bo=\frac{\rho_0.g.R^2}{\gamma_0}\sim 10^{-3} \tag{1}$$

where ρ_0 is the liquid density (1084 kg m^{-3}),[32] g is the acceleration due to gravity (9.8 N kg^{-1}) and γ_0 is the surface tension at the air-liquid interface (3.7×10^{-2} N m^{-1}). The parameter values are for methyl benzoate at standard temperature and pressure.[33]

The droplet evaporates at a velocity E_0, which is sufficiently small to ensure that creeping flow holds ($Re \ll 1$).

$$Re=\frac{\rho_0.E_0.R}{\mu_0}\sim 10^{-7} \tag{2}$$

where μ_0 is the viscosity of the liquid (1.8×10^{-3} N s m^{-2}).[32] The initial evaporation velocity, E_0, (2.0×10^{-9} m^3 m^{-2} s^{-1}) was determined by measuring the mass loss from a Petri dish containing methyl benzoate, at standard temperature and pressure. The units are converted to a volumetric basis using the liquid density.[32]

It is assumed that the substrate is flat and sufficiently wetting, such that the liquid film is thin enough to use the lubrication approximation. This assumes the vertical length scale, H, is much smaller than the horizontal one, R, $\left(\frac{H^2}{R^2}\ll 1\right)$. For a thin film, one can ignore sedimentation and assume that vertical diffusion is significant to ensure that there are no depth-wise gradients in composition.

The local evaporation velocity of the volatile liquid is E. A host of different evaporation models can be considered. We use both uniform and nonuniform evaporation. The former assumes that the evaporation velocity is the same at all locations and the latter draws on an analogy with electrostatics[26] to set a flux that increases towards the edge of the droplet. A normalization constant, k, is used to ensure the same overall rate of mass loss from the entire droplet.

$$\text{Uniform model}: E(r)=E_0 \tag{3}$$

$$\text{Non-uniform model}: E(r)=kE_0\ R^{0.5}(R-r)^{-0.5} \tag{4}$$

The polymer is assumed to have an initially homogeneous distribution, with volume fraction ϕ_0. As evaporation proceeds, the volume fraction of the polymer will increase. This

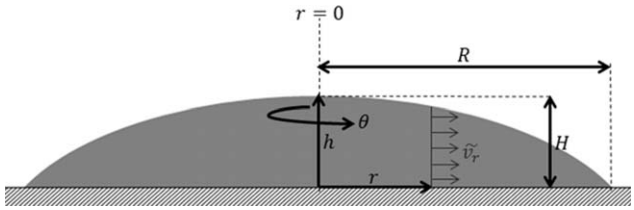

Figure 2. Sketch of a droplet.

The vertical length scale H and horizontal length scale R. In a cylindrical coordinate frame (r, h, θ). The height averaged horizontal velocity is $\bar{v}_r$.

Table 1. Scaling Terms Used

Property	Scaling Term
Air-liquid interface height, h	H
Vertical height, z	H
Horizontal position, r	R
Vertical velocity, v_z	E_0
Horizontal velocity, v_r	$R.\ E_0/H$
Viscosity, μ	μ_0
Surface tension, γ	γ_0
Density, ρ	ρ_0
Pressure, p	$\mu_0.\ R^2\ E_0/H^3$
Time, t	H/E_0

cannot happen indefinitely, therefore, a maximal value $\phi_{\max}$ is imposed, due to packing or gelling, dependent on the exact system under investigation. It is well known that the viscosity of a medium will change for different volume fractions of the dispersed material. The expression we use to account for this (following Ref. [34]), is shown in Eq. 5.

$$\mu=\mu_0\left[1-\frac{\phi}{\phi_{\max}}\right]^{-n} \tag{5}$$

The constant, n, accounts for the rate of increase in viscosity.

The surface tension of the liquid will be influenced by the presence of polymer and we account for this with the function $s(\phi)$ in Eq. 6.

$$\gamma=\gamma_0.s(\phi) \tag{6}$$

In this work, however, the effect on surface tension is minimal and we typically take $s(\phi)$ to be unity.

Shortly after evaporation commences, a close-packed region ($\phi=\phi_{\max}$) of polymer develops towards the edge of the droplet. This occurs due to the removal of liquid by evaporation and the outward capillary flow. Previous work[30,31] has assumed that evaporation is completely suppressed in this location. Here, we extend the model to account for the general case where evaporation is hindered by a fixed fraction, f_h:

$$\text{In the close-packed region}: E_h(r)=(1-f_h)E(r), \text{where } 0\le f_h\le 1 \tag{7}$$

In some contexts, horizontal diffusion of the polymer can play an important role in determining the final shape. This will depend on the diffusion coefficient of the polymer in the liquid medium. We take this into account by introducing the Péclet number ($Pé$), which is the ratio of convective to diffusive transport rates.

$$Pé=\frac{R^2.E_0}{H.D}\sim 2\times10^1-4\times10^3 \tag{8}$$

D is the diffusivity of polymer in the liquid medium (1.2×10^{-12} m^2 s^{-1}, for 100 nm rigid spheres in methyl benzoate) and H is the initial vertical extent of the droplet (typically ~ 7 μm). The experiments, to be outlined in the experimental details section, were conducted at 50−125 °C. To estimate $Pé$, we use a rule of thumb that E_0 approximately doubles for every 10 °C rise in temperature.

For practical situations, the Péclet number is typically large, therefore, our base case will be $Pé\to\infty$ (i.e. negligible diffusion) but we will also consider some cases of finite $Pé$, to predict the effect of weak diffusion.

Derivation methodology and governing equations

Previous works[30,31] have derived the governing equations for the evolution of droplet height and volume fraction of nonvolatile component. Here, we outline the derivation methodology and state the equations.

To consider transport within the droplet, it is necessary to determine the horizontal velocity. To do this, one starts from continuity and the Navier-Stokes equations. These equations are scaled, such that the nondimensional properties are indicated with an overbar, e.g., $h=H\bar{h}$ (see Table 1).

The conservation equations are simplified using the assumptions of lubrication theory, finding that the vertical pressure gradient is negligible and that the horizontal pressure gradient is related to the second derivative of horizontal velocity with respect to the vertical direction. This expression is integrated twice, subject to no-slip at the substrate and zero-shear at the air-liquid interface, to obtain an expression for the horizontal velocity as a function of the horizontal pressure gradient and vertical position.

The surface pressure is set using the Young-Laplace equation ($p=-\gamma\kappa$), where κ is the droplet's mean curvature. This is differentiated to get an expression for the horizontal pressure gradient as a function of the droplet height and its' derivatives. By substituting this into the expression for the velocity and integrating, the (dimensionless) vertically averaged horizontal velocity is found to be

$$\tilde{\bar{v}_r}=\frac{\bar{h}^2}{Ca.g(\phi)}.\frac{\partial}{\partial\bar{r}}\left[s(\phi).\left(\frac{\partial^2\bar{h}}{\partial\bar{r}^2}+\frac{1}{\bar{r}}.\frac{\partial\bar{h}}{\partial\bar{r}}\right)\right] \tag{9}$$

where $Ca=\frac{3\mu_0.R^4.E_0}{\gamma_0.H^4}$ is the capillary number and $g(\phi)=\frac{\mu}{\mu_0}$ accounts for the viscosity correction.

A mass balance produces the governing partial differential equations for droplet height and volume fraction of nonvolatile component, as

$$\frac{\partial\bar{h}}{\partial\bar{t}}=-\bar{E}(\bar{r})-\frac{1}{\bar{r}}.\frac{\partial}{\partial\bar{r}}\left[\bar{r}.\bar{h}.\tilde{\bar{v}_r}\right] \tag{10}$$

$$\frac{\partial\phi}{\partial\bar{t}}=\frac{\phi.\bar{E}(\bar{r})}{\bar{h}}-\tilde{\bar{v}_r}.\frac{\partial\phi}{\partial\bar{r}}+\frac{Pé^{-1}}{\bar{r}.\bar{h}}.\frac{\partial}{\partial\bar{r}}\left[\bar{r}.\bar{h}.\frac{\partial\phi}{\partial\bar{r}}\right] \tag{11}$$

where $\bar{E}(\bar{r})$ is the dimensionless form of the evaporation velocity profile.

It should be noted that the dynamics within the droplet are mostly controlled by the magnitude of the capillary number Ca, which is a measure of the relative importance of viscous to surface tension forces. This dimensionless group directly influences the magnitude of the horizontal velocity.

Boundary conditions and implementation

Extension to a General Treatment. At the center of the droplet, the boundary conditions are symmetry and zero

Table 2. The Ink Properties

Ink	Polymer Concentration (kg m^{-3})	Polymer Molecular Weight (kg mol^{-1})	ϕ_0	$\frac{\phi_0}{\phi_{\max}}$
A	50×10^0	1.0×10^2	5.0×10^{-3}	6.3×10^{-2}
B	1.0×10^1	1.0×10^2	1.0×10^{-2}	1.3×10^{-1}
C	1.5×10^1	1.0×10^2	1.5×10^{-2}	1.9×10^{-1}
D	2.0×10^1	1.0×10^2	2.0×10^{-2}	2.5×10^{-1}
E	5.0×10^0	2.0×10^2	5.0×10^{-3}	6.7×10^{-2}
F	5.0×10^0	5.0×10^2	5.0×10^{-3}	8.2×10^{-2}
G	5.0×10^0	7.2×10^2	5.0×10^{-3}	1.0×10^{-1}

flux. At the edge of the droplet the height is zero and the horizontal velocity is zero, such that the droplet remains pinned. A short time after evaporation commences a close-packed region ($\phi=\phi_{max}$) forms. The viscosity at this point is very large and the material behaves like a solid. The partial differential equations are now solved for the liquid domain (i.e. from the center, up to the liquid/gel front), with the height and volume fraction invariant in time between the liquid/gel front and the droplet edge. Boundary conditions at the liquid/gel front are required. The first is that the height at the liquid/gel front remains unchanged. The second sets the horizontal velocity. One way to do this is to assume that the nonvolatile component completely suppresses evaporation.[30,31] If this were the case the horizontal velocity at the liquid/gel front would be zero and residual liquid would remain in the gelled region. For the more general case, with arbitrary evaporation from the gelled region, one obtains

$$\tilde{\bar{v}_r}|_{\bar{r}=\bar{r}_f}=\frac{(1-f_h)\int_{\bar{r}_f}^{1}\bar{r}.\bar{E}(\bar{r}).d\bar{r}}{\bar{r}_f.\bar{h}_f} \tag{12}$$

No $d\bar{r}_f/d\bar{t}$ term is included because the velocity is based on a volumetric average. Generally, the integral in Eq. 12 can be evaluated numerically at each time-step. Alternatively, there is a simple analytical solution for the case of uniform evaporation. The problem also collapses to the simple, previously considered, suppressed evaporation case when $f_h=1$.

At critical polymer contents (typically $\sim \phi_0/\phi_{max} < 0.3$), that depend on f_h and the chosen evaporation model, $E(r)$, a gelled region is predicted to form at the center of the droplet, in addition to the edge. This is because the outward capillary flow acts for a longer time before the onset of gelation. This can cause the height profile to adopt negative curvature, with the smallest height in the liquid domain being at the center. The increase in polymer volume fraction then becomes largest at the center. When the gelation also occurs at the center, the solution domain gradually shrinks from both directions, since the central liquid/gel front proceeds outward. The inner boundary conditions are that height is unchanged at the central liquid/gel front and that velocity is set using a similar expression to Eq. 12, with flow being in the opposite direction and different integration limits.

Numerical Implementation. To prevent the necessity of solving a system of nonlinear equations at each time step, as per a fully implicit scheme, and to avoid stability issues that arise with explicit schemes, we use a mixed scheme.

Provided that the time-step is sufficiently small, spatial derivatives of height should change faster than the height itself. The discretised equation is solved in MatLab using Newton's method to provide an update for the height. Similarly, the volume fraction of the nonvolatile component is solved using Newton's method.

Groups that we will consider

In this article, we will examine the effects that capillary number and initial and maximal volume fractions have on the final shape. We will mention the evaporation suppression factor, Péclet number and evaporative flux distribution. These are of less interest because they cannot be altered significantly in our experiments, nor in practice.

Experimental Details

We consider flat substrates, consisting of a 150 nm layer of indium tin oxide on top of 7 mm of glass. The substrates were initially washed with acetone, followed by isopropanol, to remove greese, dust, and fingerprints. A *Litrex 80 L* inkjet printer was used to jet droplets of methyl benzoate, containing a known quantity of a typical, light emitting polymer (the nonvolatile component) used in organic light-emitting diode technologies. The jetting velocity, drop volume, and directionality are known, as are the associated errors. An array of 12 × 18 composite droplets was printed on each substrate. Immediately following jetting, the substrates were placed on a hot plate, to control the total evaporation rate. After complete drying, a *Zygo* white light interferometer was used to measure the film profiles. The measurements were post-processed to dimensionless form to enable direct comparison with each other and the numerical findings.

In an attempt to vary the magnitude of the capillary number, we used a variety of hot plate temperatures, in the range 50−125 °C and droplet volumes, $7.5\times10^{-14}-3.6\times10^{-13}$ m^3. The temperature sets the evaporation rate, E_0, and the droplet volume alters H and R.

The initial volume fraction of the polymer (ϕ_0) was varied by changing the mass of polymer in the ink. The maximal volume fraction of the polymer (ϕ_{max}) was altered by changing the polymer molecular weight. Table 2 shows a list of the inks used.

The ink viscosity, as a function of polymer volume fraction and molecular weight is shown in Figure 3. This was measured using a *TA Instruments, AR1000*, cone and plate rheometer, with a 60 mm, 1° stainless steel cone. The viscosity was obtained from extrapolation of the measured data to a shear rate of 0 s^{-1}. We fit the data in Figure 3, to Eq. 5, to determine an approximate ϕ_{max} for each polymer molecular weight.

The experimental measurements of h as a function of r should be cast into dimensionless form, to enable comparison with the numerical results. For pinned droplets, the final base width is $2R$. Assuming a spherical cap initial shape, we can estimate the initial droplet height, H from:

$$H \sim \frac{2V}{\pi R^2} \tag{13}$$

Where V is the initial droplet volume. The calculated values of H and R are then used to scale the experimental measurements. For the polymer system considered, gelation occurs at ϕ_{max}. Residual liquid in the polymer gel gradually evaporates, causing the swollen gel to shrink, until a dry film is achieved. The final experimental profiles have $\phi=\phi_f$, for the dry films. The numerical results use the gelation volume fraction $\phi=\phi_{max}$ and do not account for polymer shrinkage. To enable comparison, the experimental height is plotted as $\phi_f.\bar{h}/\phi_{max}$ against $\bar{r}$. To determine the final polymer volume fraction (ϕ_f) in each experiment, we match the initial and final polymer quantities. This is done by equating the printed droplet volume and the initial polymer volume fraction, with the product of ϕ_f and the volume integral of the final experimental profile. The camera and algorithms on the *Litrex* printer provide a measure of the volume of each ink drop ejected and the program controls the number of drops printed, and combined, into each droplet in the 12 by 18 array.

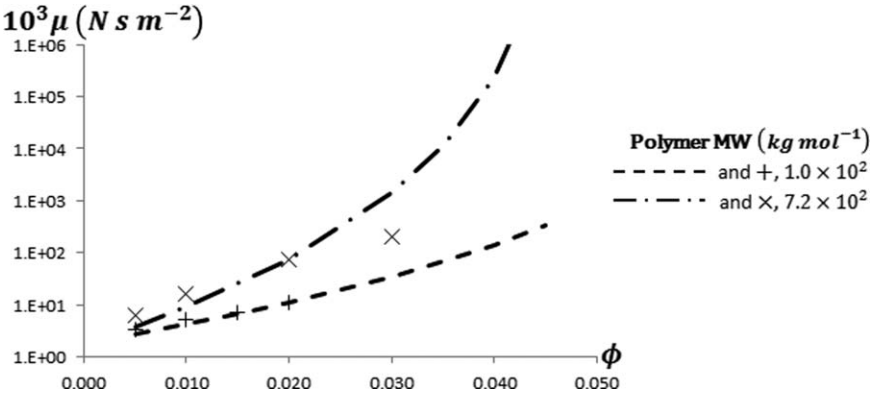

Figure 3. Viscosity as a function of polymer volume fraction and molecular weight.

The dotted lines represent the fitting to Eq. 5. The lines diverge at ϕ_{max}, which is 0.08 for 1.0×10^5 MW polymer and 0.05 for 7.2×10^5 MW polymer.

$$\phi_f = \frac{V.\phi_0}{0.5.\int_{-R}^{R} 2\pi rh.dr} \tag{14}$$

Results and Discussion

Capillary number

The final film shape is shown in Figure 4, for a range of simulations varying the capillary number. When the capillary number is large, there is minimal internal flow in the droplet, because viscous effects dominate surface tension. Consequently, no coffee-ring shape is observed. When the capillary number is small, a surface tension driven flow redistributes material, to ensure that an equilibrium shape is maintained. This flow transports the nonvolatile component toward the edge of the droplet and causes a coffee-ring shape. For intermediate values of the capillary number, we see a less pronounced coffee-ring.

The position of the liquid/gel front throughout the drying process is shown in Figure 5. Initially, the liquid/gel front propagates quickly in the large Ca case because there is no material arriving at the edge to dilute the higher polymer volume fraction. With smaller Ca, it initially takes a longer time for the liquid/gel front to propagate because the surface tension driven flow transports fluid with smaller polymer volume fraction to the edge. At later times, the liquid/gel front accelerates sharply for small Ca because the height of the droplet is smaller, causing a larger increase in volume fraction of polymer when the liquid evaporates. For $f_h=1$, as in Figure 5, the final drying time increases with increasing Ca; this is because the liquid/gel front propagation is faster and there is no evaporation from the gelled region.

Experimentally, the droplet volume and hot plate temperatures were varied. However, we estimate that for all experiments $Ca \sim 10^{-5}-10^{-2}$. The behavior is, therefore, always dominated by surface tension rather than viscous forces. For this reason, we should observe a coffee-ring in each of the experiments. This agrees with observations – no change in final shape occurred when droplet volume or hot plate temperature were changed.

Polymer volume fraction - numerical results

From the numerical solutions, the final shape was found not to change when the group ϕ_0/ϕ_{max} was kept constant. For this reason, we argue that the important group determining the residue shape is ϕ_0/ϕ_{max}, rather than any individual contribution.

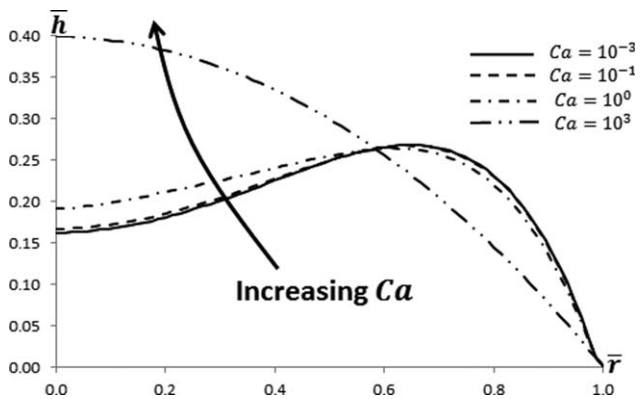

Figure 4. Numerical results: Final shape dependence on capillary number.

The results are shown for $\phi_0=0.4.\phi_{max}, f_h=1, Pé\to\infty, E(r)=E_0, g(\phi)$ using Eq. 5 and $s(\phi)=1$.

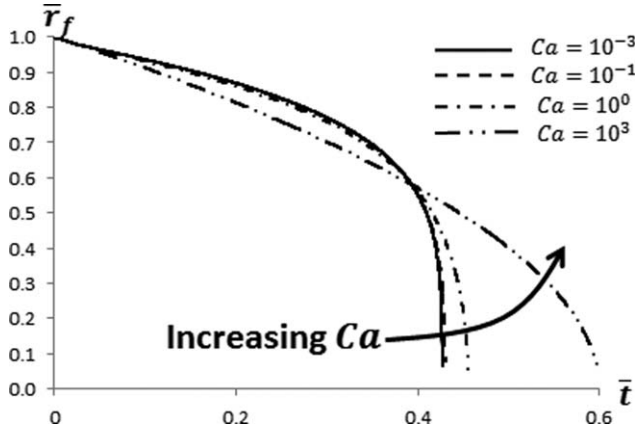

Figure 5. Numerical results: The liquid/gel front progression with dimensionless time and its' dependence on capillary number.

The results are shown for $\phi_0=0.4.\phi_{max}, f_h=1, Pé\to\infty, E(r)=E_0, g(\phi)$ using Eq. 5 and $s(\phi)=1$.

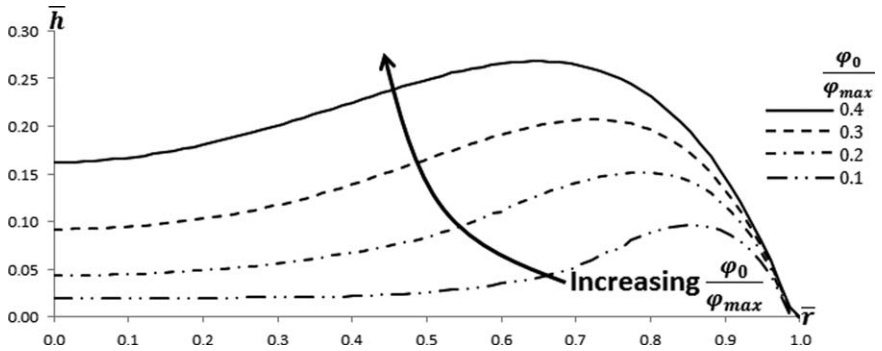

Figure 6. Numerical results: Final shape dependence on polymer volume fraction ratio ("large" values).

The results are shown for $Ca=10^{-3}, f_h=1, Pé\to\infty, E(r)=E_0, g(\phi)$ using Eq. 5 and $s(\phi)=1$.

We define the ring peak to be the maxima in the final $\bar{h}(\bar{r})$ profile and the central height to be the final height, $\bar{h}$ at the location $\bar{r}=0$. When $\phi_0/\phi_{\max}$ is large, we observe a less extreme coffee-ring shape. The ring peak is less confined to the periphery of the droplet and a significant proportion of the material is deposited centrally within the droplet. The peak ring to center height ratio is relatively small. This is shown in Figure 6.

The position of the liquid/gel front throughout the drying process is shown in Figure 7. With a large $\phi_0/\phi_{\max}$, the liquid/gel front formation and propagation are fast. With smaller $\phi_0/\phi_{\max}$ it takes more time for the liquid/gel front to propagate. The peak ring height is reduced at smaller $\phi_0/\phi_{\max}$, due to less polymer material and a corresponding, larger evaporation time. In addition, the capillary flow acts for a longer period of time before the droplet height is fixed by the formation of the liquid/gel front. The resulting final shape has a larger extent of coffee-ring formation, when normalizing peak ring height by the final central height. At later times, the liquid/gel front accelerates sharply (see Figure 7) because the height of the droplet is small, causing a larger increase in volume fraction of polymer when the liquid evaporates. The droplet can also gel in the center, when $\phi_0/\phi_{\max} < 0.3$. This results in a liquid/gel front moving outward from the center, in addition to the original liquid/gel front moving inwards from the edge. The liquid domain shrinks from both extremities.

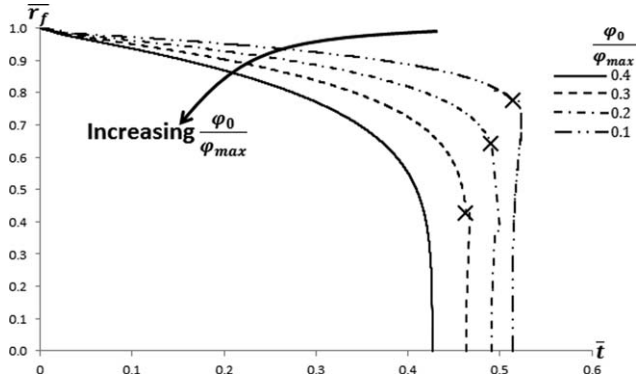

Figure 7. Numerical results: The liquid/gel front progression with dimensionless time and its' dependence on polymer volume fraction ratio.

The results are shown for $Ca=10^{-3}, f_h=1, Pé\to\infty, E(r)=E_0, g(\phi)$ using Eq. 5 and $s(\phi)=1$. The position of the original liquid/gel front when the droplet gels at the center, is indicated by the symbol ×.

As the initial polymer volume fraction ratio is decreased, the extent of coffee-ring formation is increased. The ring peak is more confined to the periphery and little material is deposited centrally within the droplet. This is shown in Figure 8. The ring height normalized by the final center height increases with decreasing $\phi_0/\phi_{\max}$, as shown in Figure 9.

If one wished to reduce the coffee-ring effect by changing the ink formulation, maximizing the polymer volume fraction ratio would be wise. Increasing this ratio decreases the ring to center height ratio. There are, however, diminishing returns on increasing the polymer volume fraction ratio. As the ratio is increased further, the improvement to film shape becomes more subtle.

Polymer volume fraction – experimental results

Altering Ink Concentration. Inks A-D were used to vary the initial polymer concentration. The experimental results are shown in Figure 10 and correspond to plots in the region of $\phi_0/\phi_{\max} = 0.1-0.3$, for the numerical solutions of Figure 6. Appropriate numerical results are superimposed for comparison. Note that the numerical results used are for a spatially uniform evaporative flux distribution and negligible polymer diffusion. Both experiments and theory show that using inks of larger polymer content results in a reduction to the coffee-ring effect when comparing peak ring to final central height ratio. It was also observed that for the experiments with the highest initial polymer loading, a raised region in the $\bar{h}(\bar{r})$ profile occurred at the center. This was significantly more pronounced than expected from the numerical solution. An interesting phenomenon discovered in the numerical solutions section, is gelation in the center, in addition to the edge, for $\phi_0/\phi_{\max} < 0.3$. This could account for a slightly larger central height than one might otherwise expect, however, it cannot explain the extent to which it occurs in practice.

Altering Polymer Molecular Weight. Inks A, E, F, and G were used to examine the effect of varying the value of $\phi_{\max}$. The experimental results for the final profile are shown in Figure 11 and correspond to plots in the region of $\phi_0/\phi_{\max} = 0.1$, for the numerical solutions of Figure 6. A polymer with larger molecular weight, has a smaller $\phi_{\max}$ (see Figure 3 and Eq. 5). It was found that using such inks reduced the coffee-ring effect. The peak ring to final central height ratio was reduced. This data supports the theory that the important group governing the final shape is $\phi_0/\phi_{\max}$

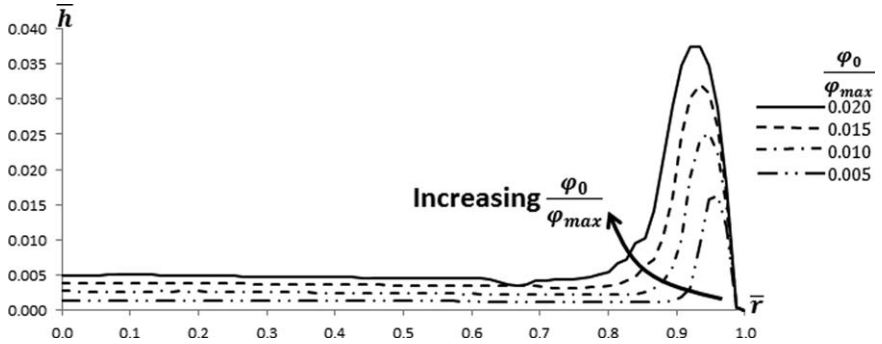

Figure 8. Numerical results: Final shape dependence on polymer volume fraction ratio ("small" values).

The results are shown for $Ca=10^{-3}, f_h=1, Pé\to\infty, E(r)=E_0, g(\phi)$ using Eq. 5 and $s(\phi)=1$.

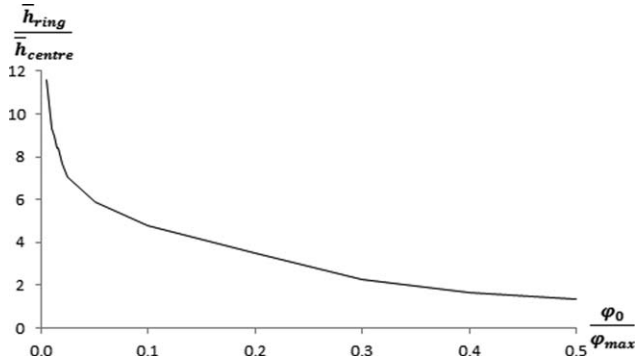

Figure 9. Numerical results: A measure for the extent of coffee-ring formation – the peak ring height normalized by the final central height, as a function of polymer volume fraction ratio.

The results are shown for $Ca=10^{-3}, f_h=1, Pé\to\infty, E(r)=E_0, g(\phi)$ using Eq. 5 and $s(\phi)=1$.

and that it should be maximized to reduce the coffee-ring behavior.

Péclet number – numerical results

When the Péclet number is reduced, diffusion of the polymer becomes progressively more important. This counteracts the transport of the polymer by the capillary flow and, therefore, coffee-ring formation is reduced. In the limit $Pé \to 0$ the coffee-ring effect is completely eliminated, as can be seen in Figure 12. For most practical inks, we estimate the Péclet number is large and does not vary to an extent that polymer diffusion is important.

Evaporation suppression factor – numerical results

Up to this point, all numerical trends have been shown for the case that $f_h = 1$. We know that no liquid remains after the droplet has dried. Therefore, there is some evaporation from the gelled region and $f_h < 1$. As shown in Figure 13,

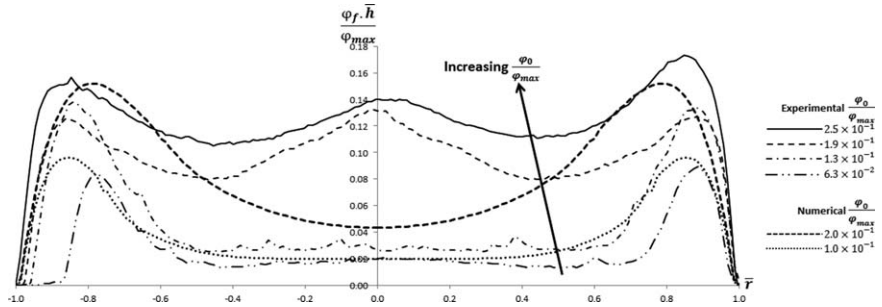

Figure 10. Experimental results: Inks A–D, varying the initial concentration of polymer.

All vertical error bars are ±10% of height. Numerical predictions are superimposed for comparison with the experiments.

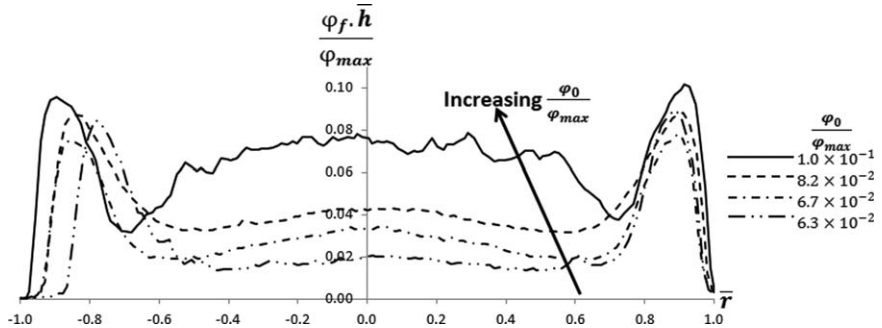

Figure 11. Experimental results: Inks A, E, F, and G – varying the polymer molecular weight.

All vertical error bars are ±10% of height.

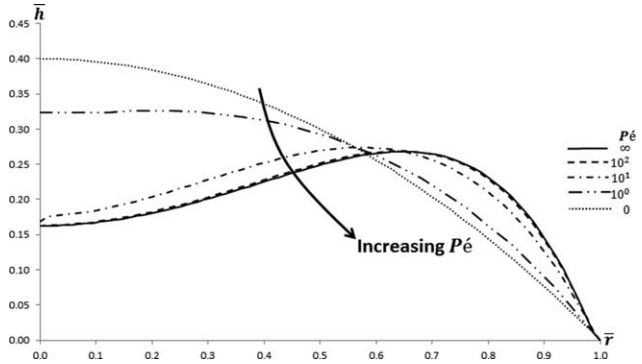

Figure 12. Numerical results: Final shape as a function of the Péclet number.

The results are shown for $Ca = 10^{-3}, \phi_0 = 0.4.\phi_{max}, f_h = 1, E(r) = E_0, g(\phi)$ using Eq. 5 and $s(\phi)=1$.

evaporation from the gelled region increases the strength of the outward capillary flow and a larger coffee-ring is observed. The peak ring height is increased, with less material deposited centrally. The polymer volume fraction ratio at which gelation occurs in the center, in addition to the edge, is larger as f_h is reduced. For example, one might expect the $f_h=0$ plot in Figure 13 to have zero material deposited at the center, due to the increased strength of the outward capillary flow. However, gelation at the center can fix the height before it decreases to that extent. This occurs even at large ϕ_0/ϕ_{max}, for small f_h.

Is the evaporative flux distribution important?

Final film profiles for the two different evaporation profiles are shown in Figure 14. With the nonuniform evaporative flux, the capillary flow is strengthened. This results in a larger coffee-ring, with a larger peak ring height and less material deposited centrally. The trends with Ca, f_h, and ϕ_0/ϕ_{max} are unchanged, however. Increasing the magnitude of Ca, the evaporation suppression factor f_h or the polymer volume fraction ratio ϕ_0/ϕ_{max} will lead to a reduction in the coffee-ring effect. This is true for both uniform and spatially varying evaporation profiles.

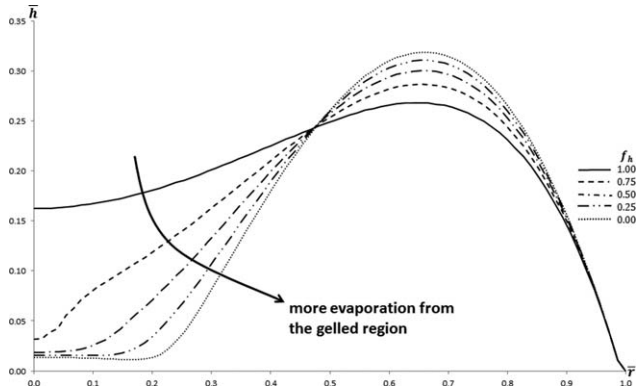

Figure 13. Numerical results: Final shape as a function of the evaporation suppression factor, f_h.

The results are shown for $Ca=10^{-3}, \phi_0=0.4.\phi_{max}$, $Pé\to\infty, E(r)=E_0, g(\phi)$ using Eq. 5 and $s(\phi)=1$.

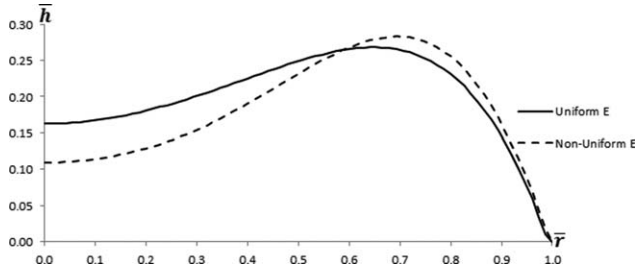

Figure 14. Numerical results: Final shape as a function of the evaporation flux distribution.

The results are shown for $Ca=10^{-3}, \phi_0=0.4.\phi_{max}, f_h=1$, $Pé\to\infty, g(\phi)$ using Eq. 5 and $s(\phi)=1$.

Conclusion

This article presents an analysis of the important groups that control the final shape of a volatile, pinned droplet, containing polymer. For all physically realizable situations, the magnitude of the capillary number is small and surface tension dominates viscous effects. Since $Ca \ll 1$, the magnitude of the viscosity, surface tension, and volatility of the liquid have little influence. The outward capillary flow, therefore, transports polymer to the edge, where it is deposited in a ring shape.

The aim of this article was to suggest means by which this ring shape could be eliminated or at least reduced. It has previously been shown that the coffee-ring formation can be suppressed by introducing surfactant driven Marangoni flow,[1] altering DLVO interactions,[18,19] using electrowetting,[21] changing particle shape[19,22,23] or through careful selection of an electric field.[20] However, none of these are ideal for P-OLED applications. In this work, we have found that the ratio of initial to maximum polymer volume fraction can be increased to decrease the ring peak to center height ratio. At large polymer volume fraction ratios, the ring height is less confined to the periphery and more material is deposited centrally. There are diminishing returns on increasing the polymer volume fraction ratio.

At critical polymer contents (typically $\sim \phi_0/\phi_{max} < 0.3$), dependent on the extent of evaporation suppression in the gelled region and the evaporation profile used, gelation is predicted to occur in the center of the droplet, in addition to the edge. For this scenario, the result would be a slightly larger central height than one might otherwise expect. This mechanism, however, cannot explain the extent to which a raised, central region appears in the experimental profiles.

The coffee-ring behavior is more extreme when evaporation is not suppressed in the gelled region at the edge of the droplet.

The exact nature of the evaporative flux distribution around the droplet may be important, although, to understand the groups controlling the behavior, it is not. The same trends exist with capillary number, evaporation suppression factor, and polymer volume fraction ratio.

In the future, this work can be extended to include solutal Marangoni effects; binary liquid systems, where the two liquid components have different volatilities and surface tensions; humidity cycling, as in Ref. [35], to periodically switch between evaporation and condensation and to analyze situations where the substrate is not flat.

Acknowledgments

This research has been funded by the Engineering & Physical Sciences Research Council, UK and CASE studentship funding from Cambridge Display Technology Ltd., UK. The authors thank Dr Mark Dowling of Cambridge Display Technology Ltd., for help with the experimental setup.

Literature Cited

1. Basi S, Hunsche M, Noga G. Effects of surfactants and the kinetic energy of monodroplets on the deposit structure of glyphosate at the micro-scale and their relevance to herbicide bio-efficacy on selected weed species. *Weed Res*. 2013;53:1–11.
2. Heim T, Preuss S, Gerstmayer B, Bosio A, Blossey R. Deposition from a drop: morphologies of unspecifically bound DNA. *J Phys Condens Matter*. 2005;17: S703–S715.
3. Angenendt P. Progress in protein and antibody microarray technology. *Drug Discov Today*. 2005;10:503–511.
4. Goldmann T, Gonzalez JS. DNA-printing: utilization of a standard inkjet printer for the transfer of nucleic acids to solid supports. *J Biochem Biophys Methods*. 2000; 42:105–110.
5. Deng Y, Zhu XY, Kienlen T, Guo A. Transport at the air/water interface is the reason for rings in protein microarrays. *J Am Chem Soc*. 2006;128:2768–2769.
6. Brutin D, Sobac B, Loquet B, Sampol J. Pattern formation in drying drops of blood. *J Fluid Mech*. 2011;667:85–95.
7. Brutin D, Sobac B, Nicloux, C. Influence of substrate nature on the evaporation of a sessile drop of blood. *J Heat Transfer*. 2012;134: 061101.
8. Sirringhaus H, Kawase T, Friend RH, Shimoda T, Inbasekaran M, Wu W, Woo EP. High-resolution inkjet printing of all-polymer transistor circuits. *Science*. 2000;290:2123–2126.
9. Kim D, Jeong S, Park B, Moon, J. Direct writing of silver conductive patterns: improvement of film morphology and conductance by controlling solvent compositions. *Appl Phys Lett*. 2006;89:264101–1-3.
10. Sekitani T, Noguchi Y, Zschieschang U, Klauk H, Someya T. Organic transistors manufactured using inkjet technology with subfemtoliter accuracy. *PNAS*. 2008;105:4976–4980.
11. Ahn BY, Duoss EB, Motala MJ, Guo X, Park SI, Xiong Y, Yoon J, Nuzzo RG, Rogers JA, Lewis JA. Omnidirectional printing of flexible, stretchable, and spanning silver microelectrodes. *Science*. 2009; 323:1590–1593.
12. Naqshbandi M, Canning J, Gibson BC, Nash MM, Crossley MJ. Room temperature self-assembly of mixed nanoparticles into photonic structures. *Nat Commun*. 2012;3:1188–1–7.
13. de Gans BJ, Schubert US. Inkjet printing of well-defined polymer dots and arrays. *Langmuir*. 2004;20:7789–7793.
14. Routh AF, Russel WB. Horizontal drying fronts during solvent evaporation from latex films. *AIChE J*. 1998;44:2088–2098.
15. Deegan RD, Bakajin O, Dupont TF, Huber G, Nagel SR, Witten TA. Capillary flow as the cause of ring stains from dried liquid drops. *Nature*. 1997;389:827–829.
16. Deegan RD. Pattern formation in drying drops. *Phys Rev E*. 2000; 61:475–485.
17. Deegan RD, Bakajin O, Dupont TF, Huber G, Nagel SR, Witten TA. Contact line deposits in an evaporating drop. *Phys Rev E*. 2000; 62:756–765.
18. Bhardwaj R, Fang X, Somasundaran P, Attinger D. Self-assembly of colloidal particles from evaporating droplets: Role of DLVO interactions and proposition of a phase diagram. *Langmuir*. 2010;26: 7833–7842.
19. Dugyala VR, Basavaraj MG. Control over coffee-ring formation in evaporating liquid drops containing ellipsoids. *Langmuir*. 2014;30: 8680–8686.
20. Wray AW, Papageorgiou DT, Craster RV, Sefiane K, Matar OK. Electrostatic suppression of the coffee-stain effect. *Langmuir*. 2014; 30:5849–5858.
21. Eral HB, Mampallil Augustine D, Duits MHG, Mugele F. Suppressing the coffee stain effect: how to control colloidal self-assembly in evaporating drops using electrowetting. *Soft Matter*. 2011;7: 4954–4958.
22. Vermant J. Fluid mechanics: when shape matters. *Nature*. 2011;476: 286–287.
23. Yunker PJ, Still T, Lohr MA, Yodh AG. Suppression of the coffeering effect by shape-dependent capillary interactions. *Nature*. 2011; 476:308–311.
24. Larson RG. Transport and deposition patterns in drying sessile droplets. *AIChE J*. 2014;60:1538–1571.
25. Routh AF. Drying of thin colloidal films. *Reports Prog Phys*. 2013; 76:046603–1–30.
26. Fischer BJ. Particle convection in an evaporating colloidal droplet. *Langmuir*. 2002;18:60–67.
27. Dunn GJ, Wilson SK, Duffy BR, David S, Sefiane K. A mathematical model for the evaporation of a thin sessile liquid droplet: comparison between experiment and theory. *Colloids Surf A Physiochem Eng Aspects*. 2008;323:50–55.
28. Maki KL, Kumar S. Fast evaporation of spreading droplets of colloidal suspensions. *Langmuir*. 2011;27:11347–11363.
29. Dehaeck S, Rednikov A, Colinet P. Vapour based interferometric measurement of local evaporation rate and interfacial temperature of evaporating droplets. *Langmuir*. 2014;30:2002–2008.
30. Ozawa K, Nishitani E, Doi M. Modeling of the drying process of liquid droplet to form thin film. *Jpn J Appl Phys*. 2005;44:4229–4234.
31. Tarasevich YY, Vodolazskaya IV, Bondarenko OP. Modeling of spatial-temporal distribution of the components in the drying sessile droplet of biological fluid. *Colloids Surf A Physiochem Eng Aspects*. 2013;432:99–103.
32. Garcia B, Miranda MJ, Leal JM, Ortega J, Matos JS. Densities and viscosities of mixing for the binary system of methyl benzoate with n-nonane at different temperatures. *Thermochim Acta*. 1991;186: 285–292.
33. Wohlfarth C. Surface tension of the mixture (1) ethanol; (2) methyl benzoate. In: Lechner MD, editor. *Supplement to IV/16, Landolt-Bornstein–Group IV Physical Chemistry*. Vol. 24; 2008:439–441.
34. Krieger IM, Dougherty TJ. A mechanism for non-newtonian flow in suspensions of rigid spheres. *Trans Soc Rheol*. 1959;3:137–152.
35. Kajiya T, Kobayashi W, Okuzono T, Doi M. Controlling profiles of polymer dots by switching between evaporation and condensation. *Langmuir*. 2010;26:10429–10432.

Manuscript received Oct. 31, 2014, and revision received Feb. 20, 2015.